

Optimization of Forged 42CrMo4 Steel Piston Pin Hole Profile Using Finite Element Method

Shaolei GAI, Jun ZHAO*, Fenghua LIN, Anhai LI, Shiying LIU

Abstract: The fatigue failure of the piston pin hole is considered as a key factor affecting the service life of engines. In this work, the piston pin hole profile was designed as tapered shape following a power law. By combining finite element analysis and hydraulic pulsating fatigue tests, the pin hole profile was optimized. It has been found that the maximum contact pressure on the pin hole surface was reduced by 16.7% with appropriate increasing the radius enlarging rate of the piston pin hole, the maximum tensile stress of the piston pin seat was reduced by 13.1%, and the piston pin seat fatigue safety factor was increased by 41.4%, the piston pin hole fatigue safety factor was increased by 15.9%. The piston pin hole's hydraulic pulsating fatigue test results were found to be consistent with the FEA results. It could be concluded that appropriate increasing the radius enlarging rate of the pin hole could significantly weaken the fatigue wear of the pin hole, further improving its fatigue resistance.

Keywords: fatigue analysis; finite element analysis (FEA); piston pin hole; profile

1 INTRODUCTION

With the increase of the explosion pressure and power of heavy diesel engines, standard aluminum-silicon alloy pistons cannot meet the technical development needs of high-explosive pressure diesel engines. Gnanavel et al. [1] mentioned that steel pistons have higher strength and fatigue resistance than aluminum pistons. In addition, steel materials have higher repeated impact resistance than aluminum alloys, therefore, the application of steel materials will be the development trend of materials for high-burst pressure and high-power diesel engine pistons [2, 3]. As an important steel material, the 42CrMo4 steel possesses some unique advantages. The experimental results by Kunc et al. [4] revealed that 42CrMo4 steel material possessed good comprehensive performance after quenching and tempering treatment. The results by Heizmann et al. [5] showed that forged 42CrMo4 steel piston possessed excellent oxidation resistance compared with other piston materials [5].

As the mechanical load and thermal load borne by the piston increase, the contact pressure on the pin hole surface of the piston also increases, which further leads to the increase of the load borne by the oil film between the pin and the pin hole. In this case, unreasonable structure of the pin hole may easily break the lubricating oil film and cause the piston failure by fatigue wear [6, 7]. Therefore, optimization design of the piston pin hole structure is of great importance to improve the fatigue resistance. Zhai et al. [8] found that the special-shaped piston pin hole structure could effectively improve its ability to withstand high burst pressure. Xiong et al. [9] found that the stress distribution at both ends of the piston pin hole could be optimized by changing the geometry of the piston pin hole, which further extended the piston life. Zhang et al. [10] mentioned that the special-shaped pin hole profile could improve the stress distribution on the piston pin hole surface, preventing the stress concentration, and reducing the risk of fatigue cracking in the piston pin hole. Ba et al. [11] conducted comparative study of the curved profile of the piston pin hole with the conical profile structure, and the results indicated that the curved profile structure led to a larger contact area between the piston pin hole and the pin, thus lowering contact friction and the resultant friction power consumption.

Cha et al. [12] mentioned that the failure of a piston was mainly triggered by the fatigue, and the fatigue crack of a piston was caused by the increase of plastic strain. Wang's et al. FEA results indicated that the maximum stress of the pin hole was located at the upper end of the hole [13]. By calculating and analyzing the stress of the piston, Liu et al. [14] established an empirical model and predicted the fatigue life. Kumar [15] established the model of a piston and investigated the thermal stress distribution of the piston under the operating condition of an engine. And the structural design of piston key parts such as pin hole using finite element analysis will help improve the high temperature performance and elevated fatigue life of diesel engine piston [16]. Buyukkaya et al. [17] and Reddy et al. [18] performed finite element analysis on the thermal performance of pistons. Havale et al. [19] and Bhagat et al. [20] used ANSYS software to optimize the piston design. According to Gogolewski et al. [21], the piston pin hole can be manufactured with a curved surface structure by using laser powder-bed fusion and machining technology. This technology can effectively improve the surface quality of the piston pin hole and improve the high-cycle fatigue strength of the pin hole.

In this paper, the model of a forged 42CrMo4 piston was established by using the finite element analyses performed to optimize the pin hole profile. The hydraulic pulsating tests on pin holes were conducted to verify the effectiveness of the optimization results of the pin hole profile.

2 MATERIAL SPECIFICATIONS OF THE FORGED STEEL PISTON

In this paper, the 42CrMo4 alloy structural steel was used as the piston material. The piston blank went through hot forging, quenching and tempering processes. Tab. 1 shows the composition of 42CrMo4 steel, and Tab. 2 shows physical properties of the steel. The metallographic structure of the 42CrMo4 steel exhibits a uniform distribution of sorbites and pearlites.

Table 1 Material composition of 42CrMo4 alloy structural steel (wt. %)

C	Si	Mn	Cr	Mo	Ni	P	S	Al	Fe
0,42	0,21	1,17	1,10	0,23	0,011	0,015	0,016	0,022	balance

Table 2 42CrMo4 alloy structural steel material physical property parameters	
Tensile strength / MPa	1006,22
Yield Strength / MPa	880,22
Elongation / %	13,88
Shrinkage / %	43,6
Young's modulus of elasticity / GPa	229,64
Poisson's ratio	0,28

3 FINITE ELEMENT SIMULATIONS AND FATIGUE TESTS

3.1 Tapered Profile of a Piston Pin Hole

Fig. 1 shows the structure of the forged 42CrMo4 piston and its pin hole profile. As shown in Fig. 1b, the segment FF is designed as a cylindrical surface with a diameter D, whereas the outer segment EE and the inner segment HH are designed as tapered holes with power law profiles.

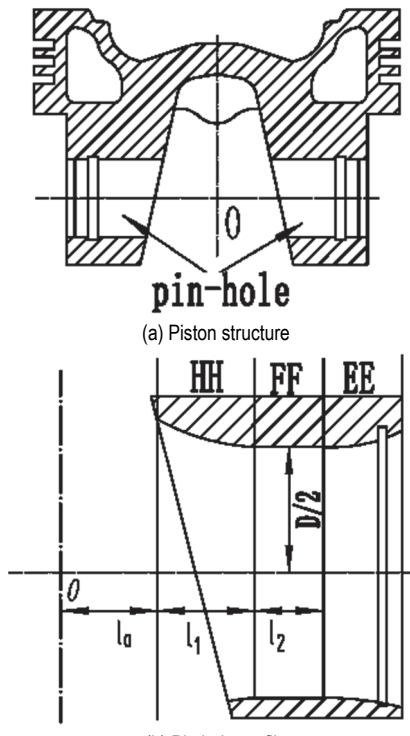


Figure 1 Structure of the forged piston and pin hole profile

The radii of segments HH and EE can be expressed by Eq. (1) and Eq. (2), respectively,

$$y = a(x - l_0 - l_1)^2 + \frac{D}{2} \quad (1)$$

$$y = b(x - l_0 - l_1 - l_2)^2 + \frac{D}{2} \quad (2)$$

where, y is the pin hole radius, a is the radius enlarging rate of segment HH, b is the radius enlarging rate of segment EE.

As is practically demonstrated, piston wear failure usually occurs on the outside of the pin hole, so the outside profile of the pin hole will be optimized, with three enlarging rates $b = 0,71 \times 10^{-4}$, $b = 1,17 \times 10^{-4}$ and $b = 1,64 \times 10^{-4}$ assigned for segment EE and a fixed enlarging rate $a = 3,33 \times 10^{-4}$ for segment HH as shown in Fig. 2.

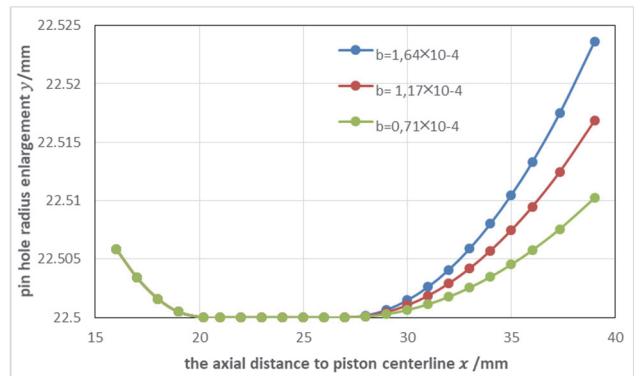


Figure 2 Piston pin hole profile

3.2 Finite Element Simulations

3.2.1 3D Modeling of Piston

A three-dimensional assembly model of the piston, piston pin and connecting rod head was established by using UG. In order to facilitate the mesh division, improve the computation efficiency while keeping sufficient accuracy, some unimportant detailed features of the piston such as the circlip grooves and the fillet of the groove bottom were ignored. Considering the symmetry of the overall structure, only one half of the piston assembly was modelled so as to reduce the calculation time.

The constructed 3D model was imported into ANSYS software for meshing and generating nodes and elements. A total of 481069 tetrahedral elements and 721209 nodes were generated for the piston and connecting rod head, meanwhile, a total of 569703 hexahedral elements and 901982 nodes were generated for the piston pin.

3.2.2 Constraint Conditions of the Piston Model

In order to ensure the uniqueness of the piston analysis results and the piston force balance, the symmetrical displacement constraint was imposed on the symmetrical section of the model as shown in Fig. 3a. The contact pairs between the piston pin and pin hole, between the pin and small end of the connecting rod, between the piston skirt and the cylinder liner are shown in Fig. 3b. The engine cylinder liner was fully restrained, and the big end of the connecting rod was fixedly restrained.

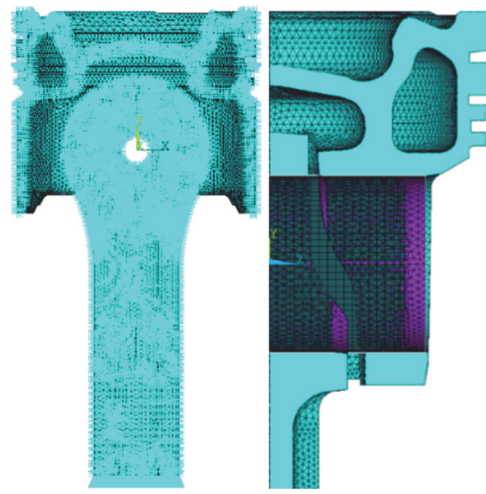


Figure 3 Piston model constraints of (a) displacement constraint and (b) contact pair

3.2.3 Piston Thermal Boundary Conditions

During the finite element simulation for the designed piston, it was assumed that the temperature distribution of the piston remains stable. The convective boundary conditions were used to calculate the temperature distribution of the piston.

Tab. 3 lists the temperatures and the heat transfer coefficients of the convective boundaries, which were obtained by the engine manufacturer after testing and calculation. The calculation results of the temperature field were applied to the nodes of the model as thermal loads.

Table 3 the test and calculated temperatures, heat transfer coefficients of the convective boundaries

Key parts of the piston	$b = 0,71 \times 10^{-4}$			$b = 1,17 \times 10^{-4}$			$b = 1,64 \times 10^{-4}$			Heat transfer / W/(m ² ·K)
	Test T / °C	Calculated T / °C	Error / %	Test T / °C	Calculated T / °C	Error / %	Test T / °C	Calculated T / °C	Error / %	
1	463	465	0,43	448	451	0,67	439	441	0,46	848
2	400	403	0,75	396	399	0,76	391	395	1,02	565
3	210	212	0,95	198	199	0,51	196	198	1,02	3164
4	154	156	1,29	151	152	0,66	149	151	1,34	804
5	333	339	1,80	322	326	1,24	316	320	1,27	3200
6	201	203	0,99	201	203	0,92	202	203	0,49	3765
7	115	116	0,87	114	115	0,88	113	114	0,88	1491
8	113	115	1,77	110	112	1,81	105	107	1,90	1798

Boundaries: 1 - Piston top, 2 - Top land, 3 - First ring groove, 4 - Second ring groove, 5 - Piston inner cold oil cavity, 6 - the piston cavity, 7 - Piston pin hole, 8 - Piston skirt

As shown in Tab. 3, the maximum relative error between the test temperature and the calculated temperature of the piston key part is 1,90%, which is within the control range of empirical error ±2%, indicating the validity and accuracy of FEM model.

3.2.4 Mechanical Boundary Conditions

During a working cycle, the piston bears the main mechanical loads such as the explosion pressure of a gas, its own inertial force and the lateral force between the piston and the cylinder liner.

Eq. (3) is the maximum reciprocating inertia force of the piston assembly

$$F_j = -m_j a \quad (3)$$

where a can be expressed by the following equation:

$$a = R\omega^2 (\cos \alpha + \lambda \cos 2\alpha) \quad (4)$$

where λ is the ratio of crank radius R to connecting rod length L .

According to the engine parameters provided by the engine manufacturer: the weight of the piston assembly m_j is 3548 g, the crank radius R is 70 mm, and the connecting rod length L is 210 mm. Rated engine speed is 2100 rpm/min. The crank rotation angular velocity ω of the engine is approximately considered as uniform because of its very small range, with its value assigned as $\omega = 2100\pi/30$ rad/s. When the crank angle α is 10°, the inertial force of the piston assembly is the largest. According to Eq. (3), the maximum reciprocating inertia force of the piston assembly F_j is -15574,41N.

The force on the top surface of the piston can be expressed by the following Eq. (5):

$$F_g = \frac{\pi D^2}{4} (P - P') \quad (5)$$

where the maximum explosion pressure of the gas on the top surface of the piston and the top land P is 23 MPa, the gas pressure of the engine crankcase P' is 0,1 MPa, and the piston diameter D is 108,4 mm. According to Eq. (5), the total force on the top surface of the piston F_g is 211233,94 N.

During the engine operating cycle, the high-temperature gas in the combustion chamber can escape into the ring groove through the gap between the piston and the cylinder. Due to the throttling, the gas pressure in the ring groove gradually decreases as the position of the ring groove moves downward. According to the experience, the gas pressure of the first ring groove and the second ring land is 76% of the gas explosion pressure. And the gas pressure of the second ring groove and the third ring land is 20% of the gas explosion pressure and the gas pressure of the third ring groove is 4% of the gas explosion pressure.

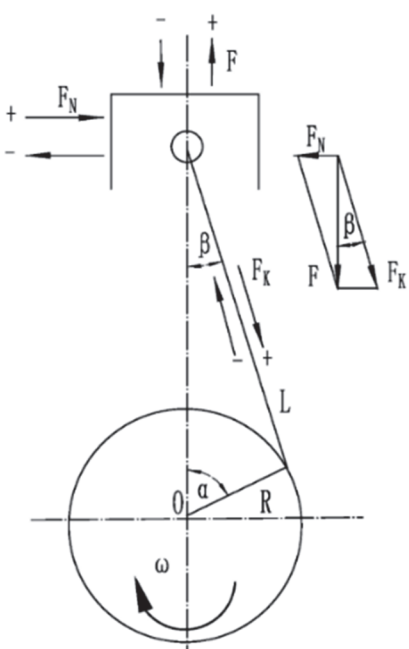


Figure 4 The force transmission in a piston

Fig. 4 shows that the total force on the top of the piston can be decomposed into the force in the connecting rod direction and the lateral force acting on the cylinder wall. The piston will also receive an equal lateral reaction force from the cylinder wall. The lateral force affects the fatigue friction loss between the piston and the cylinder liner [22, 23].

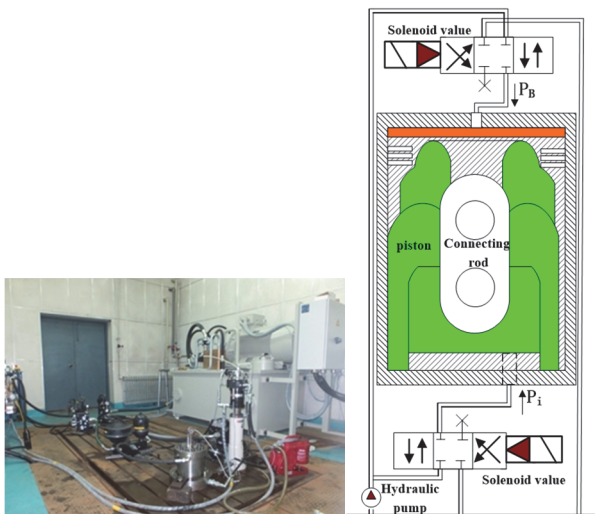
Eq. (6) expresses the lateral force on the piston as:

$$F_N = F \tan \beta \quad (6)$$

where the total force on the piston $F = F_g + F_j$ and $\beta = \sin^{-1}(\lambda \sin \alpha)$, β is the swing angle of the connecting rod. According to Eq. (6), the lateral force on the piston F_N is 11 343,75 N.

3.3 Hydraulic Pulsating Fatigue Tests of Pin Holes

Fig. 5a shows the testing setups and corresponding schematic diagram of the hydraulic pulsating fatigue. Type PP88PA hydraulic pulsating fatigue testing machine is used in the fatigue tests per the enterprise standard Q/BHS 00889-2015 [22]. The electro-hydraulic servo valve controlled by the control unit provides hydraulic power during the test. Fig. 5b shows the Sine wave loading pressure output by the servo driver.



(a) Testing setups and schematic diagram of the hydraulic pulsating fatigue

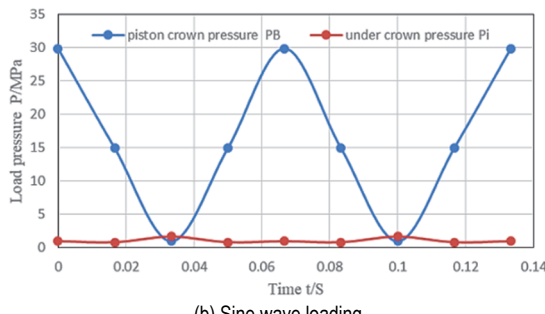


Figure 5 Hydraulic pulsating fatigue test scheme

The dynamic loading frequency during the test is 15 Hz. The maximum pressure of the mechanical load on the top of the piston is a safety value which is increased by 30% on the engine's rated maximum explosion pressure. In this work, the maximum pressure on the top of the piston is 29,9 MPa (the maximum gas explosion pressure is

23 MPa) and the minimum pressure on the top of the piston is 1 MPa. By contrast, the maximum pressure at the bottom of the piston is 1,7 MPa. The pressure phase difference between the top and bottom of the piston is 180°. It is verified whether the forged 42CrMo4 steel piston pin hole failed under 10^7 cycles of testing.

4 RESULTS ANALYSES

4.1 Contact Pressure on Pin Hole Surface

Fig. 6 shows the contact pressure distribution on pin hole surface for different radius enlarging rates of the outer pin hole profile. It can be seen that the maximum contact pressure is located on the top surface of the pin hole. For the enlarging rates $b = 0,71 \times 10^{-4}$, $b = 1,17 \times 10^{-4}$ and $b = 1,64 \times 10^{-4}$.

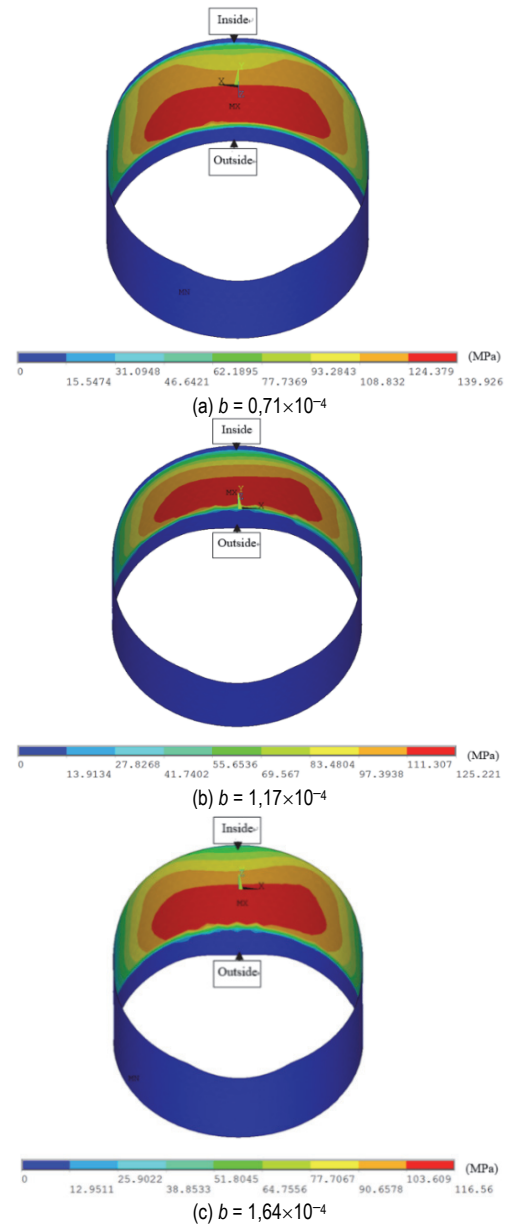


Figure 6 Contact pressure distribution on pin hole surface with different enlarging rates of outer profiles

Tab. 4 lists that the maximum contact pressure on the pin hole surface is 139,926 MPa, 125,221 MPa and 116,56 MPa, respectively. Obviously, the maximum contact pressure between the piston pin hole and the piston pin is

significantly reduced by 16,7% with appropriate increasing the radius enlarging rate of pin hole profile. This optimization of the pin hole profile increases the load-bearing area on the piston pin hole, which can further help to improve the fatigue and wear resistance of the pin hole and pin seat.

Table 4 The maximum contact pressure on the pin hole surface

Enlarging rates of the pin hole outside profile	Maximum contact pressure /MPa
$b = 0,71 \times 10^{-4}$	139,926
$b = 1,17 \times 10^{-4}$	125,221
$b = 1,64 \times 10^{-4}$	116,56

4.2 Stress Field Analysis of Piston Pin Seat

Figs. 7a and 7b show the FEM results of thermal stress field of the pistons for pin hole radius enlarging rates $b = 0,71 \times 10^{-4}$, $b = 1,64 \times 10^{-4}$. In Tab. 5, it can be seen that the piston pin seat is dominated by tensile stress, and the thermal stress gradients are 19,2378 MPa - 75,2638 MPa and 14,8007 MPa - 69,3883 MPa, respectively for the two cases. The thermal stress distribution is relatively uniform, with the maximum stress not exceeding 100 MPa, and there is no stress concentration phenomenon. The FEM results also indicate that the thermal stress of the pin seat is relatively low, and the thermal load has a relatively small effect on the fatigue performance of the pin seat.

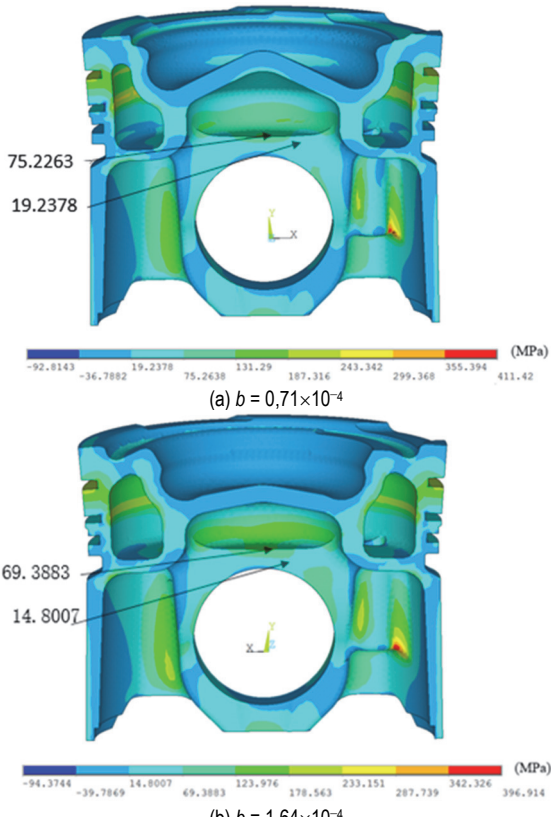


Figure 7 The thermal stress field of pistons with different pin hole radius enlarging rates

Figs. 8a and 8b show the FEM results of thermo-mechanical stress field for the above two cases. It can be seen that stress concentration occurs at the position above the outer side of the pin hole for both pin hole radius enlarging rates $b = 0,71 \times 10^{-4}$ and $b = 1,64 \times 10^{-4}$. As shown

in Tab. 5, the maximum tensile stresses are 386,5 MPa and 335,9 MPa, respectively. The FEM results indicate that the mechanical load has a significant influence on the stress field of the piston pin seat. With the increase of the outer profile enlarging rate of the pin hole, the maximum tensile stress of the pin seat is notably reduced by 13,1%. The optimized design of the pin hole reduces the risk of fatigue failure of the pin seat.

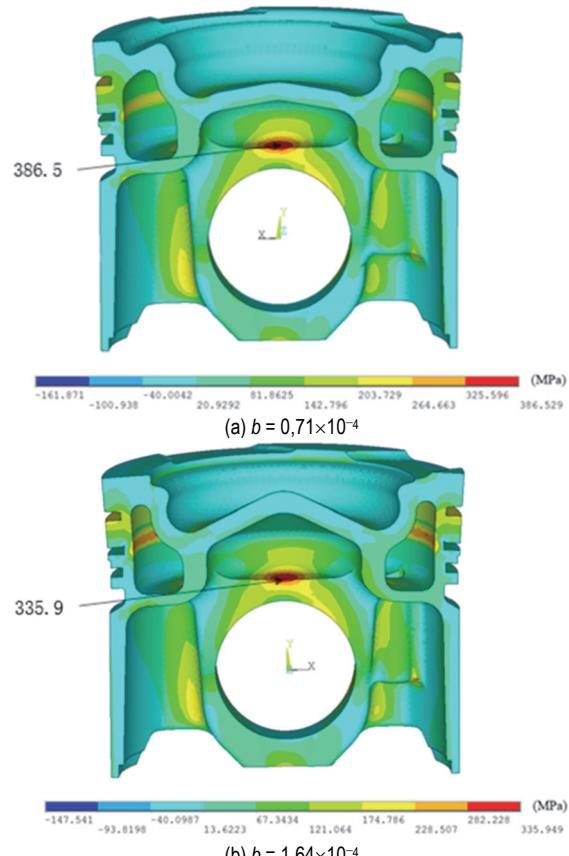


Figure 8 The thermal-mechanical stress field of pistons with different pin hole radius enlarging rates

Table 5 The thermal stress gradients of the piston pin seat and the maximum tensile stresses of the pin hole

Enlarging rates of the pin hole outside profile	Thermal stress gradients of the piston pin seat / MPa	Maximum tensile stresses of the pin hole / MPa
$b = 0,71 \times 10^{-4}$	19,2378 - 75,2638	386,5
$b = 1,64 \times 10^{-4}$	14,8007 - 69,3883	335,9

4.3 Fatigue Safety Factor

Figs. 9a to 9c show the calculated distributions of fatigue safety factors for pin hole radius enlarging rates $b = 0,71 \times 10^{-4}$, $b = 1,17 \times 10^{-4}$ and $b = 1,64 \times 10^{-4}$. The fatigue safety factors of the pin seats are 1,6797, 1,9974 and 2,375, respectively under the above three cases. The fatigue safety factors of the pin holes are 2,4375, 2,5625 and 2,825, respectively. The FEM calculation results indicate that the fatigue safety factor of the pin seat increases by 41,4%, and the fatigue safety factor of the pin hole increases by 15,9% with the increase in enlarging rate. It can be confirmed that increasing the enlarging rate of the pin hole profile can trigger a significant effect on the fatigue safety factor improvement of the pin hole and pin seat.

4.4 Hydraulic Pulsating Fatigue Tests of Piston Pin Holes

Hydraulic pulsating fatigue tests of piston pin holes were conducted along with worn surface analysis to verify the FEM calculated results. As shown in Fig. 10a, after 10⁷ cycles of the fatigue tests, severe wear marks and lubricant deposits were observed on area A (the area outside the top surface of the pin hole) of the piston with pin hole radius enlarging rate $b = 0,71 \times 10^{-4}$. However, as shown in Fig. 10b, for the piston with pin hole radius enlarging rate $b = 1,64 \times 10^{-4}$, the wear marks on area B of the top surface of the pin hole were significantly mitigated, with no lubricant deposits left on the surface.

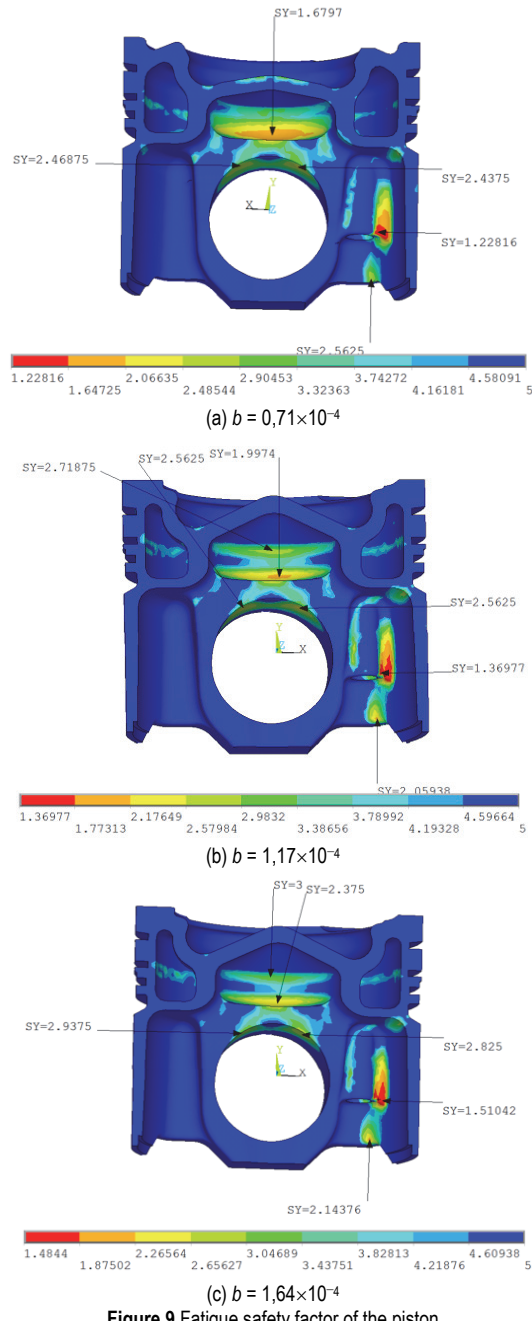


Figure 9 Fatigue safety factor of the piston

These above results are consistent with Ba's research [11] by using multi-body dynamics model and piston pin hole lubrication model, in which it is concluded that rough contact pressure of parabola contour is smaller than that of square contour, and the wear of parabola contour is

smaller. The increasing of the pin hole radius enlarging rate, the enlarging of the piston pin hole conforms to the deformation of piston pin, the contact pressure is reduced, and the wear is reduced. Therefore, the fatigue test results also indicated that appropriate increase in the enlarging rate of the pin hole radius could weaken the fatigue wear of pin hole, which provided abundant support for the FEA results.

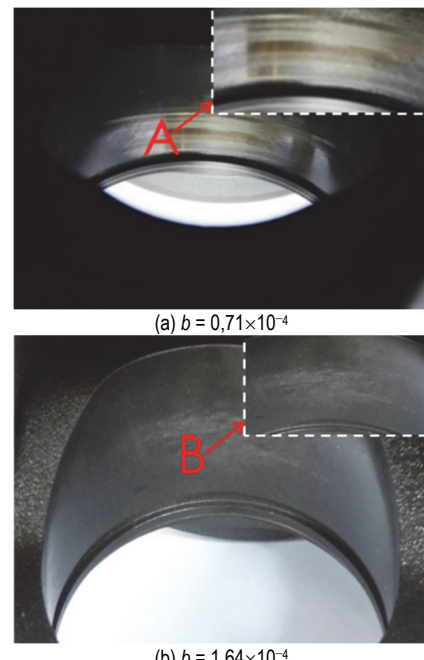


Figure 10 Fatigue wear on piston pin hole surfaces

5 CONCLUSIONS

In order to reduce the stress concentration of the piston pin seat and reduce the wear of the piston pin hole, the pin hole profile of forged 42CrMo4 steel piston is designed as tapered shape following a power law. The following conclusions can be drawn from the investigations by means of FEM calculations and hydraulic pulsating fatigue tests on piston pin holes with different radius enlarging rates.

(1) Appropriate adjusting the radius enlarging rate of the piston pin hole could control and optimize the pressure distribution on the contact surface between the pin and pin hole.

(2) Finite element analysis was carried out on the designed forged 42CrMo4 steel piston. The analysis results showed that the maximum contact pressure of the piston pin hole was reduced by 16,7% with an appropriate increase in enlarging rate of the pin hole radius. Furthermore, the maximum tensile stress of the piston pin seat was reduced by 13,1%, the fatigue safety factor of the piston pin hole was increased by 15,9%, and the fatigue safety factor of the piston pin seat is increased by 41,4%.

(3) The hydraulic pulsating fatigue test results of the piston pin hole were found to be consistent with the FEA results.

Acknowledgements

This work was supported by the Key Technology Research and Development Program of Shandong Province, China (2019JZZY010114) and the Young Scholars Program of Shandong University (2018WLJH57).

6 REFERENCES

- [1] Gnanavel, C., Saravanan, R., & Chandrasekaran, M. (2018). Investigation of appropriateness of coated steel piston for aluminium alloy piston for small engines. *International Journal of Ambient Energy*, 41(11), 1293-1298. <https://doi.org/10.1080/01430750.2018.1507945>
- [2] Schneider, S., Schreer, K., Ehnis H., & Spangenberg, S. (2014). System comparison of steel & aluminium pistons for PC diesel engines. *Auto Tech Review*, 3, 24-29. <https://doi.org/10.1365/s40112-014-0759-7>
- [3] Schreer, K., Roth, I., Schneider, S., & Ehnis H. (2014). Analysis of aluminum and steel pistons - comparison of friction, piston temperature, and combustion. *Journal of Engineering for Gas Turbines and Power*, 136(10), 101506. <https://doi.org/10.1115/1.4027275>
- [4] Kunc, R. & Prebil, I. (2003). Low-cycle fatigue properties of steel 42CrMo4. *Materials Science and Engineering: A*, 345(1-2), 278-285. [https://doi.org/10.1016/S0921-5093\(02\)00464-1](https://doi.org/10.1016/S0921-5093(02)00464-1)
- [5] Heizmann, J. & Blau, D. (2018). High-strength Pistons for Diesel Engines. *ATZ off highway worldwide*, 11, 40-43. <https://doi.org/10.1007/s41321-018-0031-1>
- [6] Suhara, T., Takei, T., & Takiguti, M. (1996). Characteristics of friction force on piston pin boss bearings. *JSAE review*, 17(4), 453. [https://doi.org/10.1016/S0389-4304\(96\)80677-1](https://doi.org/10.1016/S0389-4304(96)80677-1)
- [7] Nishikawa, C. (2012). Optimization of semi-floating piston pin boss formed by using oil-film simulations. *SAE Technical Papers*, 2012-01-0908. <https://doi.org/10.4271/2012-01-0908>
- [8] Zhai, P., Zhang, C. R., Wang, X. L., Qin, L., & Qin, Y. Z. (2018). Novel mechanism for boring non-cylinder piston pin hole based on giant magneto strictive materials. *Journal of Shanghai University (English Edition)*, 12(4), 363-367. <https://doi.org/10.1007/s11741-008-0415-1>
- [9] Xiong, P., Geng, D., Hao, G., Zhang, J., Guo, W., Zhao, W., & Chen, L. (2019). Influence of piston pin hole offset on cavity erosion of diesel engine cylinder liner. *Engineering Failure Analysis*, 103, 217-225. <https://doi.org/10.1016/j.engfailanal.2019.04.022>
- [10] Zhang, L., Lu, S., Han, Q., Liu, Z., & Zhang, W. (2017). Comparison of piston pin hole profiles for diesel engine, *Vehicle Engine*, 3, 78-81.
- [11] Ba, L., He, Z. P., Liu, Y. H., & Zhang G. C. (2015). Analysis of piston-pin lubrication considering the effects of structure deformation and cavitation. *Journal of Zhejiang University-Science A (Applied Physics & Engineering)*, 16(06), 443-463. <https://doi.org/10.1631/jzus.A1400105>
- [12] Cha, S. W., Ha, E. J., Lee, K. W., & Chang, H. (2009). Development of fatigue durability analysis techniques for engine piston using CAE. *SAE International Journal of Materials and Manufacturing*, 2(1), 403-408. <https://www.jstor.org/stable/26282771>
- [13] Wang, Y., Liu, Y., & Shi, H. (2010). Simulation and analysis of thermo-mechanical coupling load and mechanical dynamic load for a piston. *2010 Second International Conference on Computer Modeling and Simulation*, 106-110. <https://doi.org/10.1109/ICCMS.2010.131>
- [14] Liu, X. F., Wang, Y., & Liu, W. H. (2017). Finite element analysis of thermo-mechanical conditions inside the piston of a diesel engine. *Applied Thermal Engineering*, 119, 312-318. <https://doi.org/10.1016/j.applthermaleng.2017.03.063>
- [15] Kumar, K. S. (2016). Design and Analysis of IC Engine Piston and Piston-Ring on Composite Material Using Creo and Ansys Software. *Journal of Engineering and Science*, 01(01), 39-51.
- [16] Liu, T., Li, A., Zhu, C., & Yuan, W. (2022). Effect of alloying elements on surface temperature field of aluminum piston in diesel engine. *Engineering Failure Analysis*, 134, 106020. <https://doi.org/10.1016/j.engfailanal.2021.106020>
- [17] Reddy, S. S. & Kumar, B. S. P. (2013). Thermal Analysis and Optimization of I.C. Engine Piston Using Finite Element Method. *International Journal of Innovative Research in Science, Engineering and Technology*, 2(12), 7834-7843.
- [18] Buyukkaya, E. & Cerit, M. (2007). Thermal analysis of a ceramic coating diesel engine piston using 3-D finite element method. *Surface & Coatings Technology*, 202, 398-402. <https://doi.org/10.1016/j.surcoat.2007.06.006>
- [19] Havale, S. A. & Wankhade, S. (2017). Design, Thermal Analysis and Optimization of a Piston Using Ansys. *International Research Journal of Engineering and Technology*, 4, 1311-1317.
- [20] Bhagat, A. R., Jibhakate, Y. M., & Chimote, K. (2012). Thermal Analysis and Optimization of I.C. Engine Piston using finite element method. *Gas*, 2, 6207-6216. https://doi.org/10.1007/978-1-4613-8372-7_27
- [21] Gogolewski, D., Bartkowiak, T., Kozior, T., & Zmarzly, P. (2021). Multiscale analysis of surface texture quality of models manufactured by laser powder-bed fusion technology and machining from 316L steel. *Materials*, 14(11), 2794. <https://doi.org/10.3390/ma14112794>
- [22] Hou, G. & Li, A. (2021). Effect of surface micro-hardness change in multi-step machining on friction and wear characteristics of titanium alloy. *Applied Sciences*, 14(11), 7471. <https://doi.org/10.3390/app11167471>
- [23] Sun, H., Li, A., Zhou, Y. et al. (2020). Dry wear characteristics of machined ZL109 aluminum-silicon alloy surface under unidirectional and reciprocating rolling-contact friction. *Surface Topography: Metrology and Properties*, 8, 015001. <https://doi.org/10.1088/2051-672X/ab61e6>
- [24] Q/BHS 0088-2015. (2015). Performance test methods for engine piston, Shandong Binzhou Bohai piston Co., Ltd.

Contact information:

Shaolei GAI

(1) Key Laboratory of High Efficiency and Clean Mechanical Manufacture of MOE, School of Mechanical Engineering, Shandong University, 17923 Jingshi Road, Jinan 250061, China
 (2) Binzhou Bohai Piston Co Ltd, 569 Bohai 21 Road, Binzhou 256602, China

Jun ZHAO

(Corresponding author)
 (1) Key Laboratory of High Efficiency and Clean Mechanical Manufacture of MOE, School of Mechanical Engineering, Shandong University, 17923 Jingshi Road, Jinan 250061, China
 (2) National Demonstration Center for Experimental Mechanical Engineering Education (Shandong University), 17923 Jingshi Road, Jinan 250061, China
 E-mail: zhaojun@sdu.edu.cn

Fenghua LIN

Binzhou Bohai Piston Co Ltd,
 569 Bohai 21 Road, Binzhou 256602, China

Anhai LI

Key Laboratory of High Efficiency and Clean Mechanical Manufacture of MOE, School of Mechanical Engineering, Shandong University, 17923 Jingshi Road, Jinan 250061, China

Shiying LIU

Binzhou Bohai Piston Co Ltd,
 569 Bohai 21 Road, Binzhou 256602, China